The following is a version of record of the journal paper: Alinejad, N., Jung, S., Kakareko, G., & Fernández-Cában, P. L. (2023). Wind-Tunnel Reproduction of Nonuniform Terrains Using Local Roughness Zones. Boundary-Layer Meteorology, 1-22.

Wind-Tunnel Reproduction of Nonuniform Terrains Using Local Roughness Zones

Nasrollah Alinejad[1]. Sungmoon Jung[1]. Grzegorz Kakareko[1]. Pedro L Fernández-Cában[1]

Abstract

Wind-tunnel modeling of Atmospheric Boundary Layer (ABL) flows has primarily consisted of simplified (purely uniform) upwind terrain conditions. This approach is easier to carry out but may not replicate the true wind characteristics of the site. This paper proposes a method to simulate nonuniform terrains in a wind-tunnel and investigates the wind characteristics produced by the method. The proposed method employs the local roughness zones where the given terrain is divided into sub-areas with an approximately uniform roughness length. Next, each sub-area is represented in the wind-tunnel with uniform roughness elements. However, the overall upwind fetch will be composed of roughness elements of various heights. To study the wind characteristics produced by the method, nine different real-world sites were simulated in the Boundary Layer Wind Tunnel (BLWT) at the University of Florida Natural Hazard Engineering Infrastructure (NHERI) Experimental Facility (EF), using a self-configurable (automated) roughness element grid. Compared with the conventional equivalent uniform representation, similarities and differences in the longitudinal mean velocity, turbulence intensity, wind spectrum, and integral length scale profiles are reported and discussed. In particular, a significant difference was observed for the higher-order moments of the longitudinal velocity component, which indicates the need for further studies in wind loads under nonuniform terrains.

Keywords Nonuniform terrain, Roughness length, Wind characteristics, Wind-tunnel

1 Introduction

✉ Sungmoon Jung
sjung@eng.famu.fsu.edu

[1] Department of Civil and Environmental Engineering, Florida A&M University – Florida State University College of Engineering, Tallahassee, FL 32310, USA

Wind-tunnel testing is a standard method to investigate the effect of upstream surface roughness on wind loads on buildings (Fernández-Cabán and Masters, 2017; Ferreira et al., 2018). Most wind-tunnel tests on low-rise buildings have been performed using uniform roughness elements (Counihan, 1971; Deaves, 1981; Kopp et al., 2005; Wang and Stathopoulos, 2006; Zisis and Stathopoulos, 2010; Sabareesh et al., 2013). However, in reality, many built-up sites have heterogeneous terrains and exhibit various degrees of complexity. Only a limited number of tests have been conducted to study the effect of the nonuniform terrain on wind loading. Most of the research on heterogeneous terrain focused on simple roughness changes where the roughness elements change only in the wind direction while remaining uniform laterally (Panofsky and Townsend, 1963; Deaves, 1981; Wang and Stathopoulos, 2007; Lim et al., 2014). Each change in the upwind roughness disrupts the Atmospheric Boundary Layer (ABL) and deviates it from equilibrium (e.g., development of internal boundary layers). To describe the wind profile under such conditions, Deaves (1981) used the Navier-Stokes equations for the mean flow quantities, along with the concept of the internal boundary layer. Wang and Stathopoulos (2007) also formulated a model to obtain wind speed profiles for simple 2D terrain changes. Their model has an outer boundary layer and a set of internal boundary layers corresponding to each uniform patch.

To summarize, most wind-tunnel studies carried out to simulate ABL flows thus far have simplified the real-world terrains as equivalent uniform terrain or laterally uniform terrain with simple transitions. However, such simplifications could be problematic considering the complex heterogeneity of real-world terrains (e.g., see Figure 1). First, the simplified uniform terrain is influenced greatly by subjective interpretation. For example, for the terrain shown in Figure 1, if equivalent uniform terrain needs to be created, what is an appropriate roughness length z_0 when the site is composed of a lake, road, and trees? If simple transitions are used, how many transitions should be applied? Second, a uniform representation of upwind terrain in the wind-tunnel produces an equilibrium state in the boundary layer, but the equilibrium state does not hold in the real world if we have a complex terrain. The difference between the two would influence the wind characteristics, as shall be demonstrated in this paper.

Figure 1 Example of sites with different land coverages, especially with a complex immediate upwind; it is not straightforward to decide about the exposure when there is a complex terrain (Exposure B(suburban areas) and Exposure C (open terrain, airport) are based on ASCE/SEI7-16 (2017))

The objective of this paper is 1) to propose a method to simulate nonuniform terrains in a wind-tunnel, and 2) to investigate the wind characteristics produced by this method. To accomplish the objective, we performed a series of flow measurement experiments in a large boundary layer wind-tunnel on both equivalent-uniform and nonuniform upwind terrains using a self-configurable and automated roughness element grid. The proposed method employs the local roughness zones, which is explained in Section 2 along with the test setup. Section 3 presents the roughness length. Section 4 compares similarities and differences between the proposed method and conventional uniform terrain assumption. Section 5 highlights the main differences in wind characteristics due to nonuniform simulation and their implications in wind loading. And finally, in Section 6, the conclusions are summarized.

2 Test Setup

2.1 Wind-tunnel Specifications

In this study, we used the wind-tunnel facility at the University of Florida (UF). The Boundary Layer Wind Tunnel (BLWT) at UF is equipped with an automated 62 × 18 roughness grid array to simulate a broad spectrum of surface roughness conditions. Each roughness element has a 5 cm × 10 cm plan area, and the height of roughness blocks varies from 0 to 16 cm. Since each roughness block can be automatically adjusted, the upwind fetch area is nicknamed as Terraformer, covering an area of 5.4 m × 18.6 m. Point measurements of 3D (u, v, and w) velocity components of the

flow were captured using three Cobra probe sensors, which were mounted to an instrument gantry system. The Cobra probes measured three velocity components at a sampling rate of 1250 Hz. Figure 2 shows the setup of the wind-tunnel for the conducted experiments. In our tests, velocity profile measurements were taken along the BLWT centerline (y = 0 m) and at the end of the Terraformer fetch (x = 29.5 m). Thirty six velocity probes were distributed vertically along the height of the BLWT from 5–1500 mm. At each of these 36 points, the wind velocity was recorded for 1 minute duration.

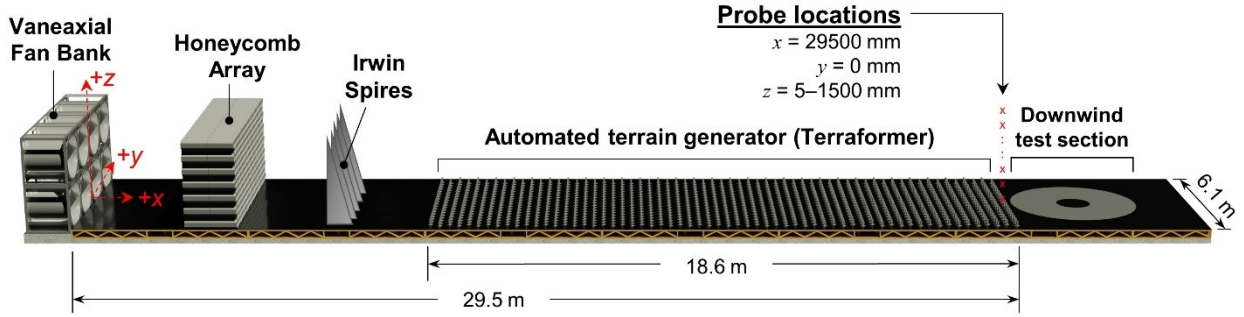

Figure 2 Schematic plan of BLWT at the UF NHERI EF

2.2 Limitation of Testing

The scale of testing for wind simulation experiments was determined such that it matches the building model scale for wind pressure testing (to be conducted in the future). The model scale was determined as 1:100 following relevant studies (Ho et al., 2005; Rizzo et al., 2012; Gavanski and Uematsu, 2014; Liu et al., 2016; Su et al., 2016) on the pressure measurements and wind characterizations. Further investigation of model scales in wind-tunnels can be found in the study by Cook (1978).

The boundary layer downwind of the measurement point affects the development of its wake, which feeds back upwind to affect the wind speed. In this study, the probe was located at a step change in roughness elements. Downwind roughness elements and surrounding buildings were not considered due to the facility restrictions, which is a common limitation in many wind-tunnels.

2.3 Implementation of Local Roughness Zones for Nonuniform Terrains

The effective roughness length is defined such that a representative uniform terrain has the same surface shear stress as the real nonuniform terrain. By employing previous studies on effective

roughness length and local roughness zones (Fiedler and Panofsky, 1972; André and Blondin, 1986; Taylor, 1987; Mason, 1988; Vihma and Savijärvi, 1991; Wieringa, 1993; Macdonald et al., 1998; Millward-Hopkins et al., 2011), any nonuniform terrain can be divided into smaller zones with uniform roughness length.

The proposed method to simulate nonuniform terrains in the wind-tunnel is as follows. First, select aerial images of real-world sites. Second, identify sub-sections with similar land coverages. In order to avoid subjective interpretation, the given site is mechanically divided as long as certain sub-section has the same characteristics (e.g., trees, roads). Third, assign the local z_0 for each sub-section. Based on the literature, most land coverages have a range of z_0. For example, short grass areas in the literature range between z_0 = 0.001 m and 0.03 m. Instead of subjectively interpreting the land coverage, three different values are considered for the local z_0: the minimum, average, and maximum. Fourth, in the wind-tunnel, set the height of the roughness elements corresponding to the roughness length for these sub-sections. Many researchers proposed equations to find the height of roughness elements in wind-tunnels, in which Lettau's equation (Lettau, 1969), Counihan's equation (Counihan, 1971), simplified Counihan's equation (Counihan, 1971), and Macdonald's equation (Macdonald et al., 1998) are most commonly used.

2.4 Selection of Terrains

We chose nine representative sites to include different terrain characteristics: smooth-to-rough transition, rough-to-smooth transition, and mixed-upwind terrains. These sites were chosen from about 60 sites that experienced the passage of actual hurricanes (Balderrama et al., 2011; Fernández-Cabán and Masters, 2017). In the site selection process, we ensured that we had different immediate upwind roughness types. The geographical location and upwind roughness classification for each site are summarized in Table 1, where the last column indicates the clockwise angle from the (magnetic) north direction. The criterion for upwind roughness classification was based on whether the final change was rough-to-smooth or smooth-to-rough, because the zone of upwind influence is roughly 600 – 300 m in full-scale (Wang and Stathopoulos, 2006; Zisis and Stathopoulos, 2010), which in 1:100 scale would be about 1/3 of the

length of the wind tunnel. Figure 3 shows the aerial images of the selected sites. The red dot at the bottom of these images is the measurement point in the wind-tunnel testing.

Table 1 Information on the nine sites simulated in the wind-tunnel

Site name	Immediate upwind Roughness type	Town	Latitude	Longitude	Wind Direction
Site 1	Rough-to-smooth	Punta Gorda, FL	26.9065	-82.0057	70
Site 2	Rough-to-smooth	Houma, LA	29.6487	-90.6940	350
Site 3	Rough-to-smooth	Stuart, FL	27.1889	-80.2411	320
Site 4	Smooth-to-rough	Satellite Beach, FL	28.1937	-80.6056	330
Site 5	Smooth-to-rough	Steinhatchee, FL	29.6731	-83.3798	300
Site 6	Mixed	Bonita Spring, FL	26.3304	-81.7791	50
Site 7	Mixed	Somers Point, NJ	39.3208	-74.5953	90
Site 8	Mixed	Naples, FL	26.1557	-81.7211	110
Site 9	Mixed	Charleston, SC	32.7141	-79.9664	150

Figure 3 Aerial images of the selected sites, respectively from left to right: site 1 to site 9 (flow direction from top to bottom)

For each of the nine terrains, real-world images were manually processed, sub-areas were identified, and three different values were assigned for the local z_0 to each sub-area: the minimum, average, and maximum, based on Table 2. These are denoted as Max, Avg, and Min, respectively, which will be used later in figures and discussions of the following sections.

Table 2 Terrain classifications and z_0 range (z_0 range is based on Davenport, 1960; Vihma and Savijärvi, 1991; Wieringa, 1993; Wang and Stathopoulos, 2007; He et al., 2017)

Terrain code	Terrain description	z_0 range (m)
T1	Water (River, sea, lake, etc.)	0.0001-0.0005

T2	Featureless Land	0.001-0.005
T3	Road	0.0024-0.03
T4	Short Grass	0.001-0.03
T5	Low-rise Building	0.3-0.7
T6	Forest	1- 2.3

In this study, to compute the height of roughness elements, we used Macdonald's equation (Eq.1), since it was known to be more accurate for sharp-edged cubes in the intermediate area densities (Macdonald et al., 1998), the situation we had in this research.

$$\frac{z_0}{H} = \left(1 - \frac{d}{H}\right) \exp\left[-\left\{0.5 \frac{C_D}{\kappa^2} \left(1 - \frac{d}{H}\right)^{-0.5}\right\}\right] \quad (1)$$

where H is the height of the roughness element, C_D is the drag coefficient, which is equal to 1.2 based on the face of a cube over shear flow, κ is von Kármán's constant, and $\frac{d}{H} = 1 + \Phi^{-\lambda}(\lambda - 1)$, where λ is the total plane area of the whole array of obstacles over the total area of upwind fetch, which is equal to 0.0555 in the UF's BLWT, and Φ is a constant parameter equal to 4.43 for staggered configuration of roughness elements (Fernández-Cabán and Masters, 2017). Figure 4 shows the roughness element heights under Avg configuration for nine sites.

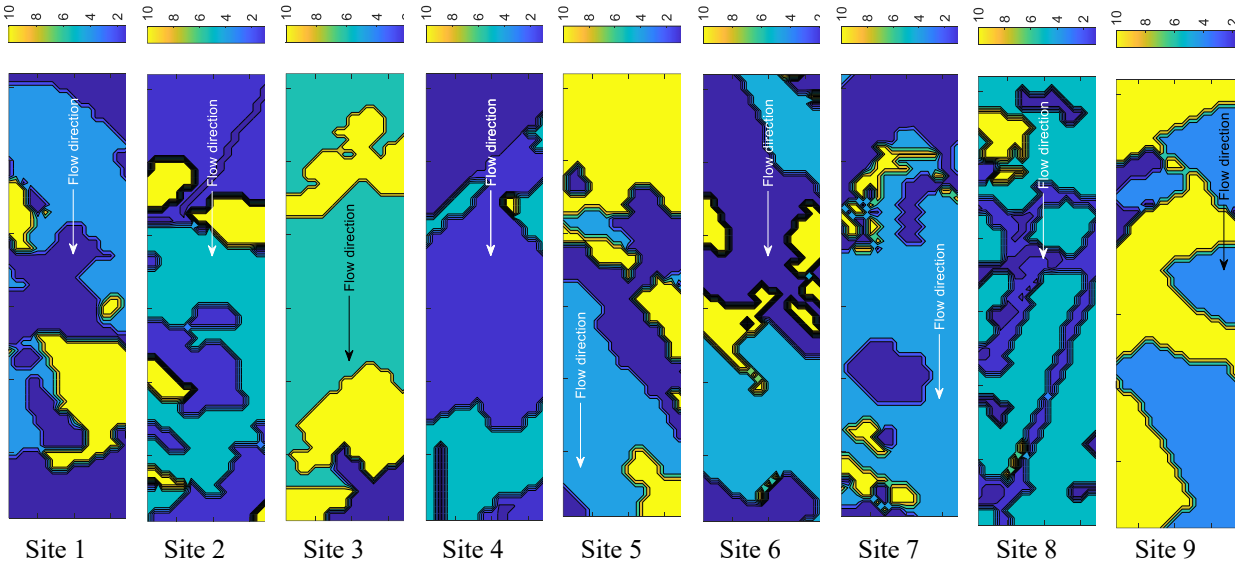

Figure 4 Roughness element heights (cm) in the wind-tunnel for sites 1 to 9, respectively from left to right, under Avg configuration

An example wind-tunnel representation of real-world nonuniform terrain is shown in Figure 5,

where the aerial image was divided into several zones with the same land coverage (Figure 5a), then based on Table 2 and Eq.1, the height of roughness elements was estimated and the map of roughness height was created (Figure 5b). Finally, the map was introduced to the wind tunnel to simulate the upwind terrain (Figure 5c).

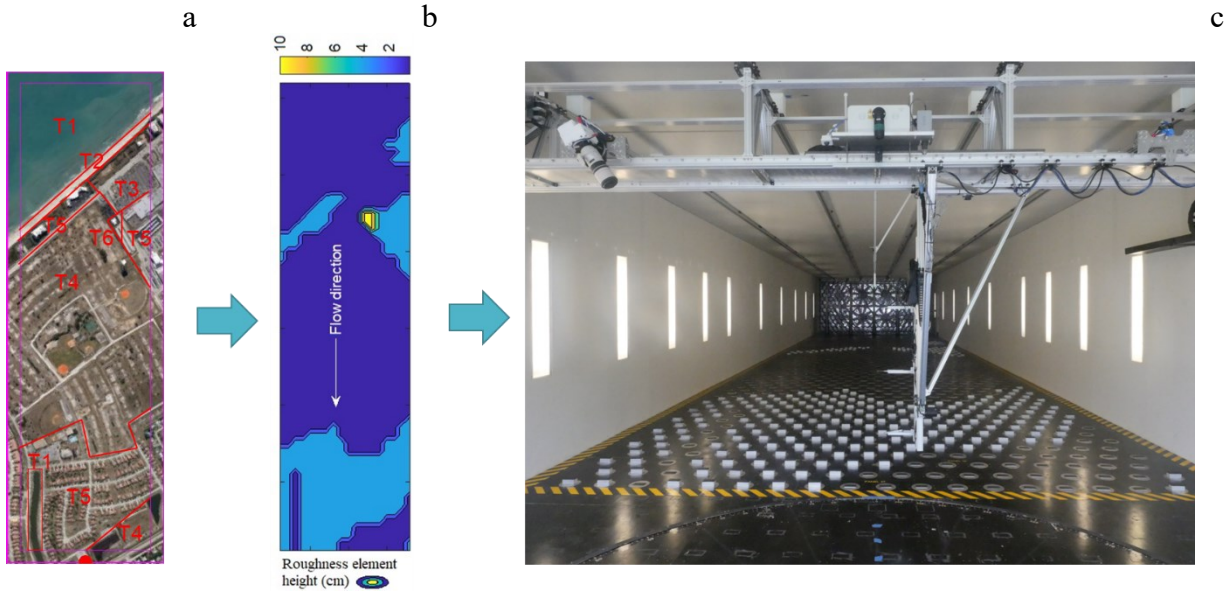

Figure 5 Producing a nonuniform roughness configuration corresponding to a real terrain and its simulation in the wind-tunnel; a) aerial images of site 4 with different land coverages zones, b) roughness element height map in cm simulated in the wind tunnel and c) wind tunnel simulation of upwind terrain for the mentioned site

In order to compare the effect of nonuniform terrain with uniform terrain on wind characteristics, we also tested 30 different uniform terrains in the range of H = 0.65 cm to 16 cm. Further details of all nonuniform and uniform sites are discussed in the following section.

3 Roughness Length Estimation

Although effective z_0 alone is not a full characterization of a site, it is still a useful parameter because a nonuniform terrain is difficult to describe. We will use the z_0 values to discuss and plot the results in the next sections. We used the logarithmic mean velocity profile (Eq.2) to compute z_0 for all upwind terrains using the wind speed measurements from the wind-tunnel.

$$z_0 = (z - d)\exp\left(-\frac{U_z\,\kappa}{u_*}\right) \quad (2)$$

In Eq.2, u_* is friction velocity, and z is the height at which the mean wind speed, U_z, has been read and d is zero-plane displacement height (Fernández-Cabán and Masters, 2017).

For each terrain in the BLWT, instead of direct estimation of zero-plane displacement height (d) from wind speed profile, we used the logarithmic wind speed profile (Eq.2) and the wind measurements at 2 different heights and solved the system of equations for two unknown variables, z_0 and d. The wind speed time series collected at 5, 10, 15 and 20 m full-scale (50, 100, 150, and 200 mm in the wind-tunnel) were used for that matter. Three pairs of measurement heights, including 5 and 10 m, 15 and 10 m, and 20 and 10 m were considered to solve Eq.2 for z_0 and d. Each pair's estimated z_0 and d were then averaged to obtain the final z_0 and d. For $z_0 < 0.15$ m, zero-plane displacement height was considered to be zero (Fernández-Cabán and Masters, 2017). The friction velocity in Eq.2 was measured using Reynolds Shear Stress Extrapolation (RSSPE) method described in Catarelli et al. (2020).

3.1 Uniform upwind terrain

The z_0 estimations for uniform upwind terrain with respect to the height of roughness elements are plotted in Figure 6. As shown in Figure 6, Eq.1 from Macdonald et al. (1998) overestimated the z_0. Thus, we used the estimated z_0 to plot and discuss the results later for both uniform and nonuniform cases. The trend line of z_0 vs. H (uniform height of roughness elements) can be used to convert z_0 values to the height of roughness elements in the UF's BLWT.

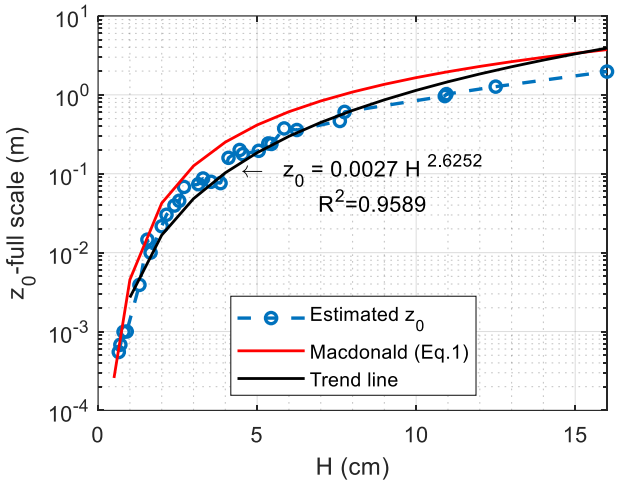

184

185 **Figure 6** Estimated z_0 (full scale equivalent) for 30 uniform BLWT upwind terrain configurations

186 **3.2 Nonuniform upwind terrain**

187 After implementing the local roughness zones method and simulation of nonuniform upwind
188 terrains in the BLWT, the z_0 was estimated for all nine sites. In Figure 7a, the estimated z_0 for all
189 nonuniform cases is plotted. The sites are classified into three groups based on their immediate
190 upwind type and ordered in an increasing z_0 fashion. Using the trend line in Figure 6, the
191 corresponding heights of roughness elements in the uniform configurations are also plotted in
192 Figure 7b to compare with the nonuniform configurations.

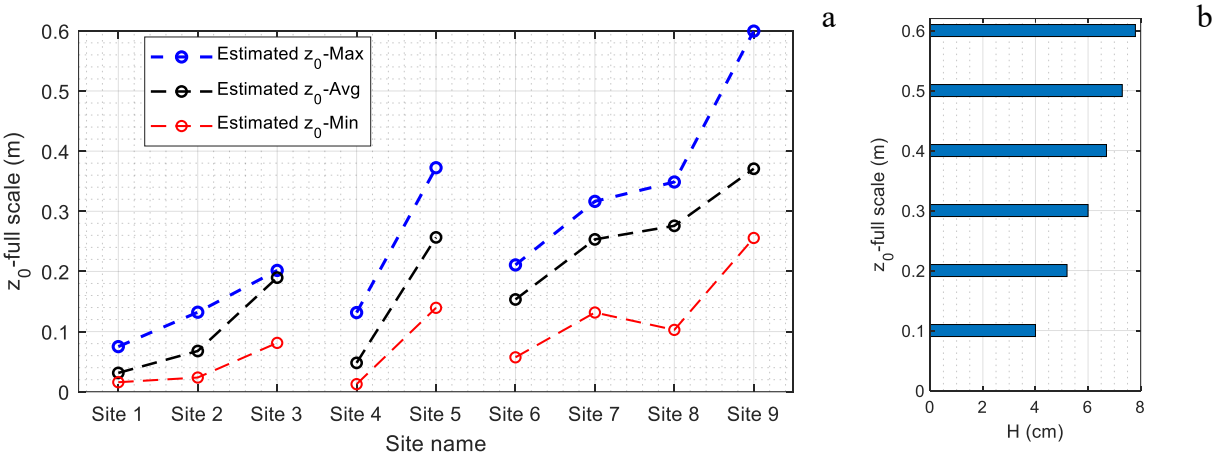

193

194 **Figure 7** a) Estimated z_0 (full scale equivalent) for nine sites with nonuniform BLWT upwind terrain configurations
195 and b) the height of the uniform roughness element configuration (H) that produced the corresponding z_0 values

4 Wind Characteristics

4.1 Wind Speed Profile

The mean wind speed profile has been calculated based on a 1-minute average of collected data at every measurement height in the wind-tunnel testing. Figure 8 shows a representative mean velocity profile for the nonuniform terrain configuration corresponding to site 6. Two different normalized log-law wind profiles were also added to Figure 8. For this site, the normalized mean wind speed at 100 mm height (10 m in full scale) (U_{10}/U_{ref}) for the Max configuration was about 6 and 14 % smaller than the Avg and Min configurations, respectively (Figure 8). Moreover, the longitudinal wind speed profile of site 6 under Min configuration with z_0 = 0.05 m was close to the log-law profile with the same z_0 near the ground (z ≤ 30 m). For example, at 10 m and 20 m heights in full scale, the normalized mean wind speed under Min configuration was only 5 % and 3%, respectively, smaller than the normalized wind speed of the log-law curve with z_0 = 0.05 m. The same pattern was also observed for the Max configuration of site 6 with z_0 = 0.21 m and the corresponding log-law profile, where the difference between the normalized longitudinal wind speed at 10 and 20 m full scale heights was about 10 % and 3 %, respectively.

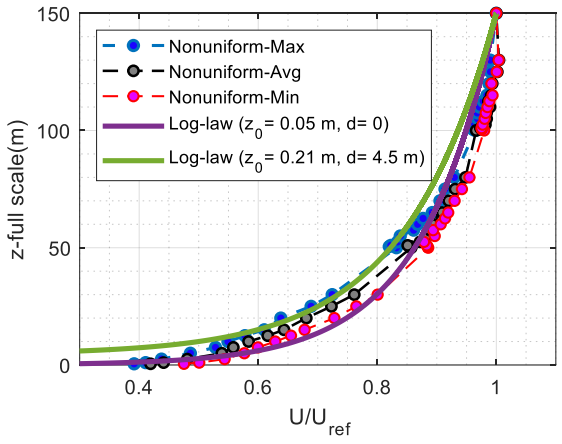

Figure 8 Comparison of mean longitudinal wind speed for three different nonuniform terrain configurations (site 6). The x-axis is the mean longitudinal velocities at each measurement height normalized by the mean value at z = 1500 mm (150 m in full scale and Uref = U (z =150 m)) and the y-axis is the full-scale converted measurement heights (measurement points in the wind-tunnel divided by the scale factor = 1/100).

In order to understand how the nonuniform representation influences the wind shear compared with the uniform approximation, we obtained U/U_{10} in Figure 9 for sites with two different immediate upwind terrain types (sites 3 and 5) since the field data were available at 5 and 10 m heights. In Figure 9, the small black dotted data shows the Florida Coastal Management Program (FCMP) field measurements at 10 and 5 m full-scale heights extracted from Gurley et al. (2021) based on their corresponding immediate upwind roughness (data from rough-to-smooth sites vs. site 3; data from smooth-to-rough sites vs. site 4). The FCMP data used to compare with the wind tunnel data are summarized in Table 3. For each FCMP site, the wind speed time series were segmented into 10-minute samples. These sites were selected based on the immediate upwind roughness type and relatively close z_0 to the wind tunnel measurements. The last column of Table 3 is based on the Davenport classification of effective roughness in ASCE/SEI7-16 (2017).

Table 3 Information on FCMP sites (Gurley et al., 2021) used to compare with the wind tunnel measurement

Storm Name, Year, Tower Index	Immediate upwind Roughness type	GPS Coordinates	Wind Direction (°)	10-minute Samples	Visual interpretation of z_0
Lili, 2000, T0	Rough-to-smooth	30.2146, -92.0447	205	57 to 108	Exposure B, z_0 = 0.25 to 0.5 m
Ivan, 2004, T1	Rough-to-smooth	30.4793, -87.1869	65	1 to 75	Exposure B, z_0 = 0.25 to 0.5 m
Rita, 2005, T3	Rough-to-smooth	29.9548, -93.9542	5	1 to 34	Exposure B, z_0 = 0.25 to 0.5 m
Ike, 2008, T1	Rough-to-smooth	29.6578, -95.0727	90	98 to 111	Exposure B, z_0 = 0.25 to 0.5 m
Ike, 2008, T2	Rough-to-smooth	29.811969, -94.901578	120	73 to 120	Exposure B, z_0 = 0.25 to 0.5 m
Gustav, 2008, T1	Smooth-to-rough	29.5831, -90.7252	0	38 to 87	Exposure B, z_0 = 0.25 to 0.5 m
Gustav, 2008, T4	Smooth-to-rough	29.5880, -90.7377	180	1 to 75	Exposure B, z_0 = 0.25 to 0.5 m
Ike, 2008, T0	Smooth-to-rough	29.7200, -95.3371	110	100 to 142	Exposure B, z_0 = 0.25 to 0.5 m

When the terrain changes from rough terrain to smooth terrain, Deaves (1981) noted that the surface shear stress would undershoot its final equilibrium value due to the sudden change and the wind speed increases near the surface. Therefore, the wind speed near the surface in a rough-to-smooth transition should be greater than that of the equivalent uniform terrain. Thus, as observed in Figure 9a, although both nonuniform and uniform cases had the same z_0, the nonuniform case had greater wind speed at 5m height than the uniform representation. The same pattern between uniform and nonuniform configurations also happened for sites 1 and 2. Moreover, the proposed

nonuniform representation had a much better match to the field data than the uniform representation. However, it is important to mention that for sites 1 and 2, the comparison with the field data is inconclusive since sites 1 and 2 had smaller z_0s than the field measurements. On the other hand, when there is a smooth to rough roughness change, the shear stress increases suddenly to above its equilibrium value due to the sudden change in roughness (Deaves, 1981). This initial increase in shear will decrease the wind speed near the ground compared with the equivalent uniform. Therefore, in Figure 9b, the nonuniform case has a lower wind speed at 5 m than the uniform case with the same z_0.

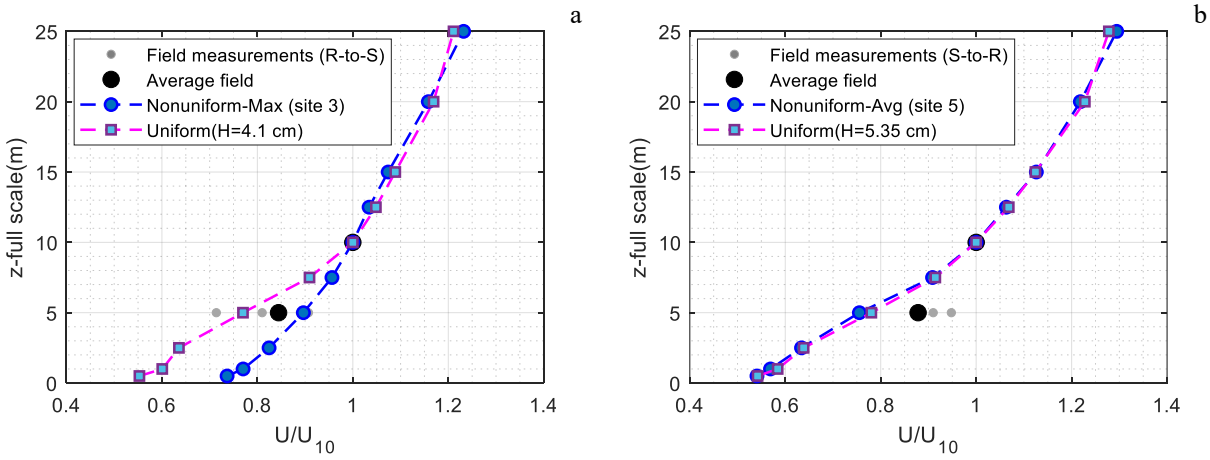

Figure 9 Normalized longitudinal wind speed profile for a) site 3 for Max configuration with z_0 = 0.2 m, uniform case with similar z_0 and field measurements with rough to smooth change; and b) site 5 for Avg configuration with z_0 = 0.26 m, uniform case with similar z_0 and field measurements with smooth to rough change. The large dots show the average of different field data.

4.2 Turbulence Intensity

The vertical profile of wind turbulence intensity, $I_u(z)$, is related to the standard deviation of the fluctuating wind components, $\sigma_u(z)$, and the mean wind speed, U_z, as:

$$I_u(z) = \frac{\sigma_u(z)}{U_z} \quad (3)$$

For nonuniform terrain configurations, the turbulence intensity increased as the height of roughness elements increased, as expected. For example, it is apparent from Figure 10 that the turbulence intensity at z = 100 mm for site 4 under the Max configuration was 13 and 34 % greater than Avg and Min configurations, respectively.

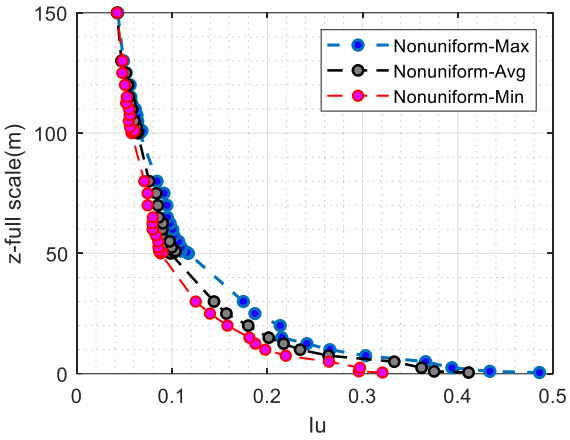

Figure 10 Comparison of wind turbulence intensity for three different nonuniform terrain configurations for site 5 at different heights above the ground

Counihan (1975) stated that turbulence intensity at 30 m "should be free from very local influences but still be representative of the local terrain." Thus, he proposed Eq.4 to show the variation of turbulence intensity versus effective roughness length for the reference height of 30 m.

$$I_u = 0.096 \log_{10} z_0 + 0.016 (\log_{10} z_0)^2 + 0.24 \quad (4)$$

Along with the turbulence intensity at 30 m, we will also show the turbulence intensity at the standard height of 10 m above the ground. The turbulence intensity at 30 and 10 m full-scale heights for all test cases (nonuniform and uniform) was obtained and plotted in Figure 11. The plots are excellent confirmation of Counihan's reasoning as well as his model's accuracy — for nonuniform terrain cases, the Counihan model provided a good trend of the turbulence at the 30 m full-scale height. However, the error was significant for some sites, with increasing order when the roughness height changed from Min, Avg, to Max. In addition, the model underestimated the turbulence intensity for uniform sites of high z_0. The high turbulence intensity of the uniform sites of high z_0 may be the artifact of the wind-tunnel testing, i.e., the use of rectangular roughness elements. As noted by Counihan, the turbulence intensity at the 10 m height was further influenced by the local features. The model prediction was much smaller than the measurements at 10 m height since Eq.4 was originally derived for a height of 30 m above the ground.

Although we observed the increasing trend of turbulence intensity by increasing the z_0 values in the uniform cases, here we discuss why the local fluctuation in the trend for nonuniform cases was observed. We have used several alphabetical labels (e.g., K, L, M, N, P, Q, R, S, X, Y) instead of

the site names and configurations in the following figures to facilitate the discussion of results. Each of these label will be explained in this section or section 5. In Figure 11a, considering points K which shows site 4 (z_0 = 0.05 m), and L which shows site 2 (z_0 = 0.07 m) both under Avg configuration, it is apparent that these points did not follow the trend locally since we see a decrease in the turbulence intensity by the increase in z_0 value. Here, it is necessary to investigate the immediate upwind roughness configuration for both sites to find the reason. As mentioned in the second column of Table 1, the final patch of roughness elements in site 2 (point L) was smooth, while the final patch in site 4 (point K) was rough. Since the final patch affects the turbulence intensity near the ground, it was expected to observe smaller turbulence intensity where there was a smooth final patch. As we go up in the elevation, farther roughness patches from the measurement point should be analyzed to figure out the local fluctuations in the turbulence intensity for the site with the same or close z_0s.

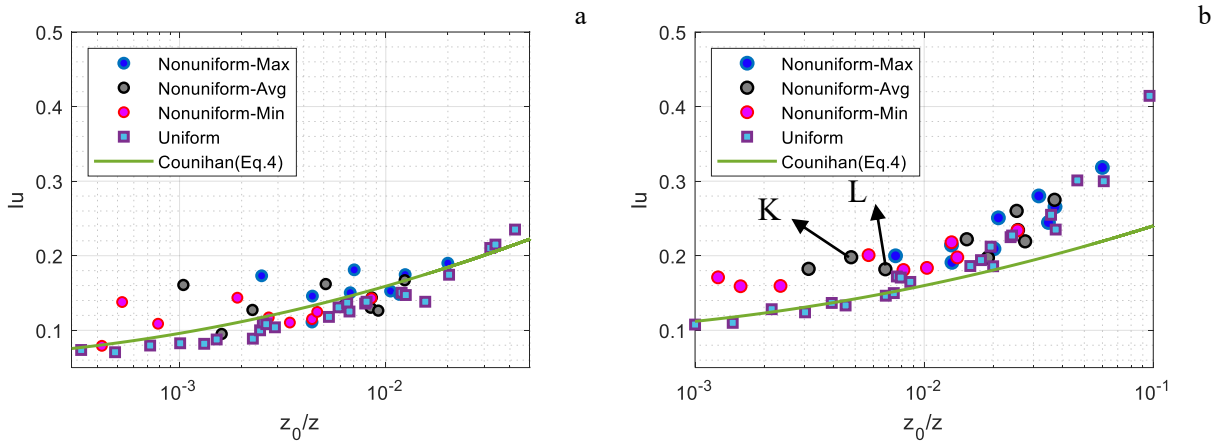

Figure 11 Wind-tunnel turbulence intensity for all test cases (nonuniform and uniform) vs z_0/z from wind-tunnel measurements a) at z = 30 m height and b) at z = 10 m height and turbulence intensity from Counihan's proposed curve (Eq.4)

The FCMP field measurements of turbulence intensity in Gurley et al. (2021) were used to further discuss the influence of immediate upwind terrain. The analysis of results showed that for rough to smooth upwind terrain sites (sites 1 to 3) and mixed upwind terrain sites (sites 6 to 9) the nonuniform representation performed better than the uniform representation. For example, in Figure 12a, at 10 m height, the turbulence intensity of nonuniform representation was about 15 % smaller than the average field-measured turbulence intensity, while the turbulence intensity of uniform representation was about 25 % smaller than the average field-measured turbulence intensity. For sites 4 and 5 with smooth to rough immediate upwind terrain, we observed that

nonuniform representation performed slightly better than nonuniform representation at 10 m height, as shown for site 5 in Figure 12b, where the turbulence intensity of nonuniform and uniform configurations were 0.234 and 0.227, respectively, compared with the average field-measured turbulence intensity which was 0.262.

Another important observation from Figure 12 is that site 3 had smaller turbulence intensity than site 5 near the surface, both under Max configurations. This phenomenon happened because the turbulence intensity near the surface is highly affected by the final patch of roughness elements (the nearest zone to the measurement point). Thus, for site 3, where the final patch of roughness elements was smooth, a smaller turbulence intensity near the ground was observed than site 5, where the final patch of roughness elements was rough. For example, the turbulence intensity of site 3 under Max configuration at 5 m height above the ground was 0.22, where the z_0 is 0.2 m. On the other hand, for site 5 under Max configuration, where the z_0 is 30 % larger than site 3 under Max configuration, the turbulence intensity at 5 m height was 63 % larger.

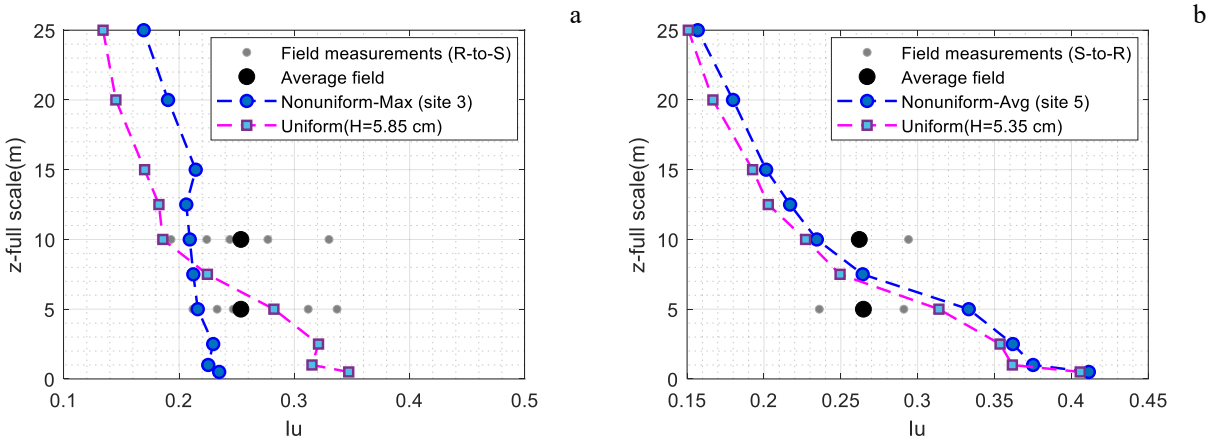

Figure 12 Turbulence intensity for a) site 3 for Max configuration with z_0= 0.2 m, uniform case with similar z_0 and field measurements with rough to smooth change; and b) site 5 for Avg configuration with z_0 = 0.26 m, uniform case with similar z_0 and field measurements with smooth to rough change. The large dots show the average of different field data.

4.3 Power Spectrum

The spectral density of turbulent kinetic energy illustrates how energy distributes across different eddy sizes (Li et al., 2012). In the low-frequency ranges (large eddies), the eddies gain energy from the mean flow and lose energy to smaller eddies. Conversely, in the high-frequency ranges (small eddies), the eddies tend to dissipate energy (Tieleman, 1995; Jung and Masters, 2013).

The power spectrum of measured data in BLWT was compared with the Engineering Sciences Data Unit (ESDU) empirical model described by Eq.5 (ESDU 74030, 1974).

$$\frac{nS_{uu}}{\sigma_u^2} = \frac{4f}{(1+70.8f^2)^{5/6}} \quad (5)$$

where n is the frequency in Hertz, S_{uu} is the power spectrum for the longitudinal turbulence component and $f = nL_{ux}/U_z$ in which L_{ux} is the longitudinal integral length scale.

Figure 13 shows the wind spectrum of two uniform configurations with different z_0s. Figure 14 shows the power spectrum of two different nonuniform sites with the same z_0. Compared with the theoretical ESDU spectrum model (Eq.5), a good agreement with the experimental results was observed in both Figure 13 andFigure 14. In Figure 13, in the high-frequency region, we observed that smoother upwind terrain had a larger normalized spectrum response. At $f = nL_{ux}/U_z = 10$ for H= 0.7 cm (Figure 13a) $\frac{nS_{uu}}{\sigma_u^2} = 0.045$ and for H= 4.55(Figure 13b) $\frac{nS_{uu}}{\sigma_u^2} = 0.037$. In Figure 14, although both sites 2 and 4 under Max configurations had the same z_0, we observed different response at high- frequency region. Site 2 with smooth immediate upwind terrain showed a larger spectrum response than site 4 with rough immediate upwind terrain in the high-frequency region. For example, at $f = nL_{ux}/U_z = 10$ for site 2 under max configuration (Figure 14a) $\frac{nS_{uu}}{\sigma_u^2} = 0.038$ and for site 4 under max configuration (Figure 14b) $\frac{nS_{uu}}{\sigma_u^2} = 0.034$. Thus, unlike uniform cases, for nonuniform cases, besides z_0, the configuration of immediate upwind terrain also played a role in the spectral densities.

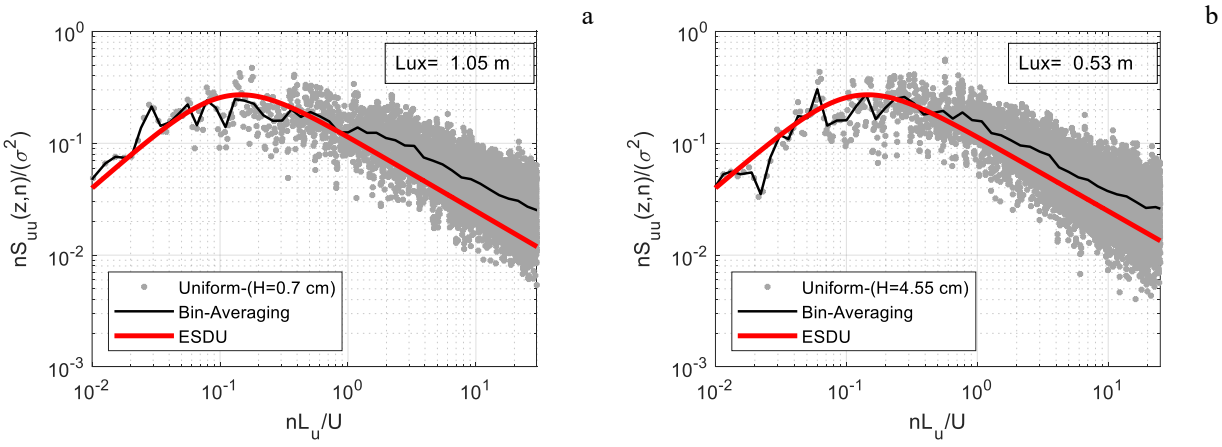

Figure 13 Power spectrum of uniform configurations at z = 10 m full-scale height for a) z_0 = 0.00007 m full-scale, b) z_0 = 0.2 m full-scale. The solid black curve shows the bin-averaging of the wind-tunnel power spectrum.

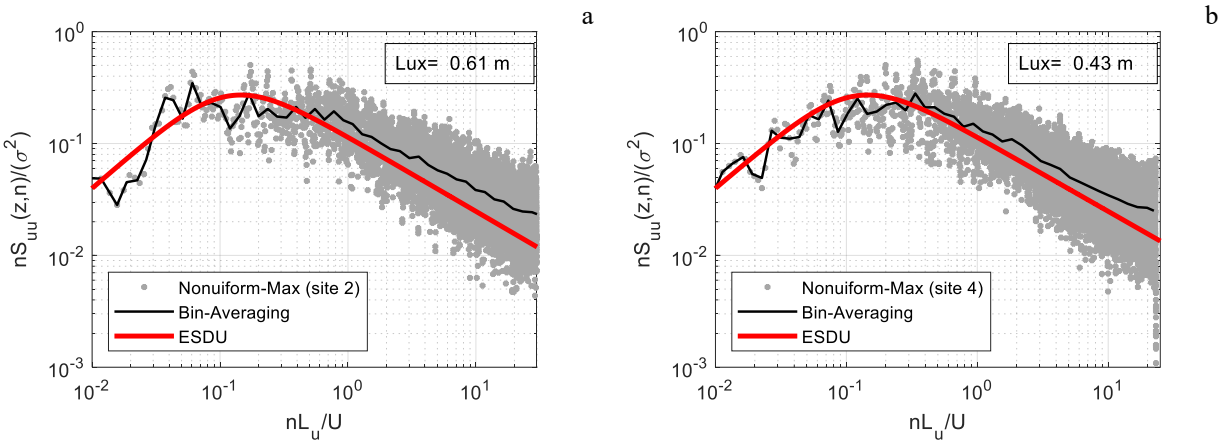

Figure 14 Power spectrum of nonuniform configurations at z = 10 m full-scale height with the same z_0 = 0.13 m full-scale for a) site 2 and b) site 4. The solid black curve shows the bin-averaging of the wind-tunnel power spectrum.

4.4 Integral Length Scale

The longitudinal integral length scales were calculated by obtaining the area under the autocorrelation function of the fluctuating velocity component multiplied by the mean wind speed at each height (Varshney and Poddar, 2011).

Many researchers (Counihan, 1975; Farell and Iyengar, 1999; Kozmar, 2010, 2011) expressed that large eddies cannot be fully developed due to limitations in the dimension of the wind-tunnel. Thus, the increase in the integral length scales with height in the full-scale experiments has not been observed in the higher elevations (z > ~50 m full scale) in the wind tunnel testing.

The length scale showed the behavior expected from the turbulence intensity plots shown earlier. In high z_0, the turbulence intensity of the uniform cases was greater than the nonuniform cases (Figure 11). As it is apparent in Figure 15, where we plotted the integral length scale at 10 m full scale height for all nonuniform and uniform cases, at the high z_0 range, the autocorrelation function peak was not as wide, so it decreased toward zero more rapidly and led to a smaller turbulence length scale for the uniform case. On the other hand, at low-to-mid z_0, length scales for some uniform cases were greater than the nonuniform, whereas for other cases were less. The general trend is that the integral length decreased by increasing z_0. Although, the fluctuation in the results at 10 m height is significant. For some cases, such as site 4 under Max configuration with z_0 = 0.13 m (Point M in Figure 15) and site 6 under Avg configuration with z_0 = 0.15 m (Point N in Figure 15), the fluctuation in the results could be the effect of immediate upwind terrain. For site 4 under

Max and site 6 under Avg configurations, the height of roughness elements in the final patch was 6.4 and 1.45 cm and the normalized integral length scale (L_{ux} / z) was 4.3 and 5, respectively. Although both sites had close z_0, the smoother final patch for site 6 made the autocorrelation function peak wider, resulting in a larger integral length scale.

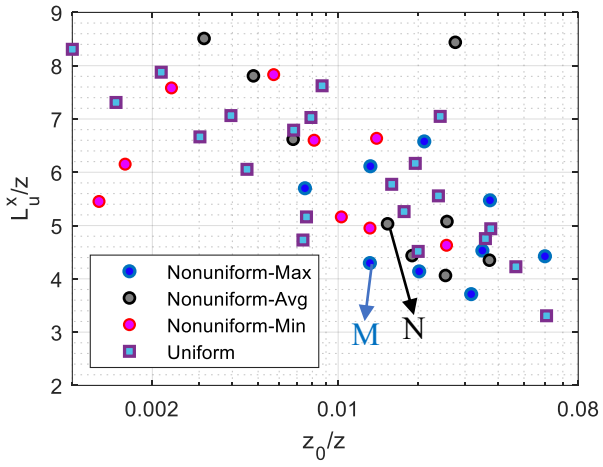

Figure 15 Wind-tunnel integral length scale for all test cases (nonuniform and uniform) vs. z_0/z from wind-tunnel measurements at z = 10 m full-scale height

After estimating the integral length scale, mentioning the integral time scale (eddy turn-over time) is important. The integral time scale (L_{ux} / U) at 1500 mm above the ground in the wind tunnel was about 0.02 sec for all cases (the maximum and minimum of integral time scale at 150 m height in full scale were 0.026 and 0.017, respectively). Since the testing duration was 60 seconds, the number of cycles in our testing would be 60 / 0.02 = 3000 cycles on average. The integral time scale at 1500 mm in the wind tunnel (150 m in full scale) did not show a considerable fluctuation in different cases because the effect of upwind terrain was negligible at this height. However, the integral time scale near the ground was highly affected by the upwind terrain. For instance, at 10 m in full scale height, the integral time scale for site 6 under Max configuration was 0.06 sec, while for site 3 under Max configuration was 0.035 sec, although both sites had similar z_0.

5 Wind Characteristics Due to Nonuniform Simulation of Roughness

5.1 Higher Order Central Moments

382 The distribution of near-surface winds in atmospheric boundary layer flows is commonly assumed
383 as the Gaussian, regardless of surface roughness characteristics. However, relatively rougher
384 terrain such as plant canopies and suburban areas has shown to exhibit non-zero skewness in the
385 wind velocities (Shaw and Seginer, 1987; Oikawa and Meng, 1995). The non-Gaussian trend in
386 the wind over suburban terrain has also been quantified for the hurricane wind records collected
387 between 1999 and 2016 (Balderrama et al., 2012; Fernández-Cabán and Masters, 2017). In both
388 analyses, a positive non-Gaussian wind speed distribution in the skewness of the longitudinal
389 velocity component was evident. Similarly, the positive skewness of tropical cyclone winds has
390 been observed by other researchers in the past decade (see the list by Xiao and Hong (2022)).

391 Positive skewness indicates the likelihood of a greater gust compared with the Gaussian
392 assumption (Balderrama et al., 2012). Therefore, it will be important to reproduce the positive
393 skewness in the wind-tunnel to obtain the peak wind loads.

394 The skewness and kurtosis at 10 m height were computed for all test cases (nonuniform and
395 uniform) and plotted in Figure 16 and Figure 18. First, the uniform roughness elements were not
396 able to reproduce the positive skewness observed in the field, except for very high z_0. This
397 observation is consistent with a previous study (Fernández-Cabán and Masters 2017, Figure 11).
398 Compared with the previous study, this research showed a slight negative bias of the skewness.
399 Second, for the most part, the proposed method of nonuniform terrain simulation was able to
400 produce positive skewness in suburban terrain ($z_0 > 0.15$ m). As the terrain became smoother ($z_0 \approx$
401 0.1 m), the skewness decreased and the wind record became closer to Gaussian. For very low z_0,
402 negative skewness was observed for most configurations. In general, the skewness decreased as
403 the z_0 decreased, however, there were some fluctuations depending on the configuration of
404 immediate upwind roughness elements. For instance, considering Points P and Q which show sites
405 9 and 3 under Min configurations, respectively, it is apparent that the skewness decreased as z_0
406 increased for these two sites. The reason for this reverse behavior is that site 3 (point Q) had a
407 smooth final patch leading to a smaller skewness compared with site 9 (point P), with a rougher
408 final patch. Third, the skewness produced in the wind-tunnel with the proposed method was
409 between about -0.2 to 0.16 at the 10 m full-scale height. This skewness is less than what was
410 observed in the records of Atlantic hurricane winds (about 0.17 to 0.42).

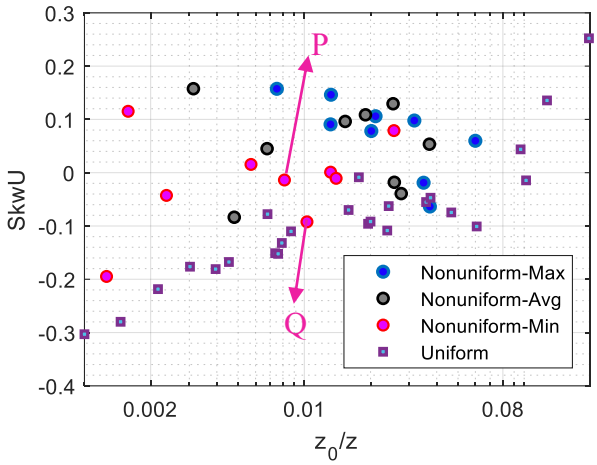

411

412 **Figure 16** Wind-tunnel skewness for all test cases (nonuniform and uniform) vs z_0/z from wind-tunnel
413 measurements at z = 10 m full-scale height

414 Fernández-Cabán and Masters (2017) provided skewness profiles for field measurements based
415 on the FCMP dataset in the suburban areas where z_0 changes between 0.15 and 0.7 m. In Figure
416 17, the skewness from field measurement was compared to the wind-tunnel measurement from
417 this study. The skewness profile of nonuniform cases in the low z_0 range (Figure 17a) and high z_0
418 range (Figure 17b) were closer to the field data than the uniform representation in the wind-tunnel.
419 For example, at 10 m height, for z_0 = 0.2, the skewness of the nonuniform and uniform cases were
420 0.08 and -0.09, while the lower and upper bounds of field measurement were 0.17 and 0.42,
421 respectively.

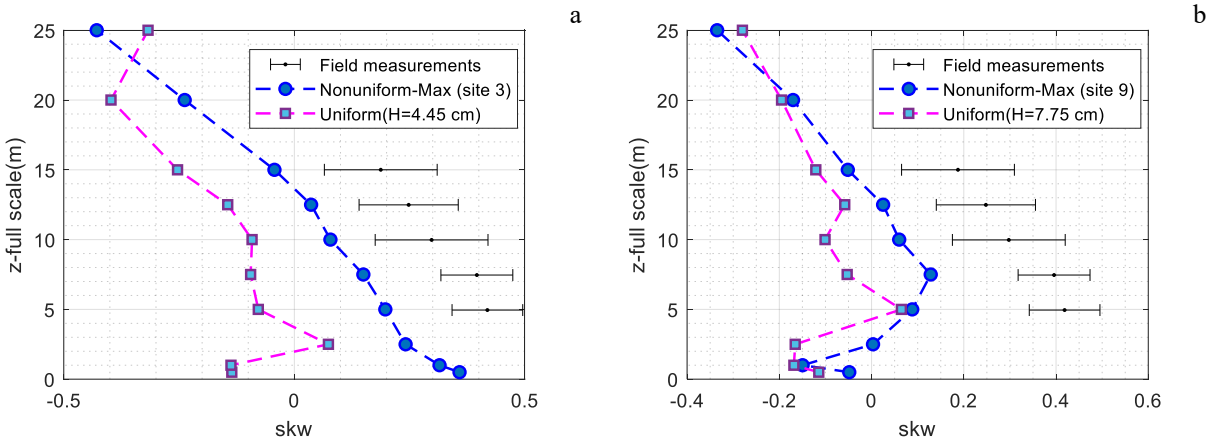

422 **Figure 17** Skewness profile in the field vs. wind-tunnel measurements for a) z_0 = 0.2 m and b) z_0 = 0.6 m in full
423 scale

The previous studies of hurricane winds showed that the kurtosis was approximately Gaussian for the suburban terrain whereas slightly platykurtic (< 3) for the open terrain (Balderrama et al., 2012; Fernández-Cabán and Masters, 2017). The kurtosis observed in this study was further platykurtic than the analysis of field data (Figure 18). The kurtosis for high and low z_0 ranges was closer to Gaussian distribution, while for mid z_0 ranges (z_0 between 0.05 and 0.5 m) was around 2.6 (<3) for both uniform and nonuniform cases. Therefore, the likelihood of greater gust will be less due to this platykurtic trend which can offset the effect of positive skewness on the extreme values partially.

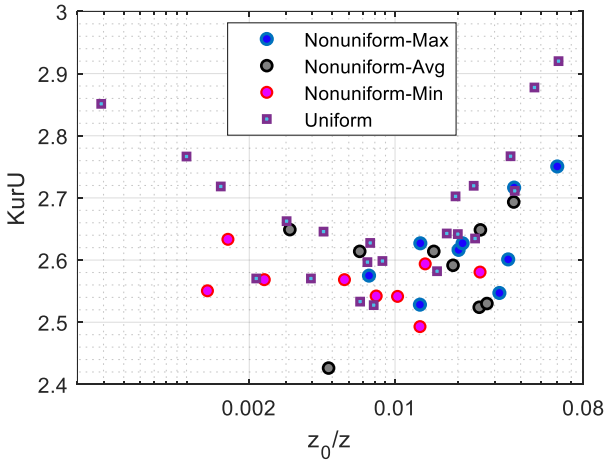

Figure 18 Wind-tunnel kurtosis for all test cases (nonuniform and uniform) vs. z_0/z from wind-tunnel measurements at z = 10 m full-scale height

5.2 Friction Velocity

The friction velocity was computed using Eq.6 and the three velocity components measured in the wind-tunnel.

$$u_* = \left(\overline{u'w'}^2 + \overline{v'w'}^2\right)^{1/4} \tag{6}$$

In Eq.6, as defined earlier, $u' = u - \bar{U}$ where u is the longitudinal wind speed component. Similarly, $w' = w - \overline{W}$ and $v' = v - \bar{V}$ are the vertical and transverse fluctuating (mean-removed) components of wind velocity. Also, $\overline{u'w'}$ and $\overline{v'w'}$ are the temporal average between the two fluctuating components (Weber, 1999).

Figure 19 shows the obtained friction velocities for all test cases (nonuniform and uniform) at 10 m full scale height. Overall, a linearly increasing trend was observed as expected, with some fluctuations in the uniform roughness cases due to the uncertainties in the testing. The main source of these uncertainties for uniform cases came from the freestream longitudinal wind velocity (U at 1500 mm in the wind tunnel) produced in the wind tunnel, which on average, was 19.6 m/s but with a ±5 % fluctuation. The nonuniform cases overall also showed a linearly increasing trend, but some points showed significantly greater or lower friction velocity than the uniform cases. Upon analysis of the sites, all these cases could be explained by a sudden change in the immediate upwind terrain. Four representative cases, points R, S, X and Y, are further explained below.

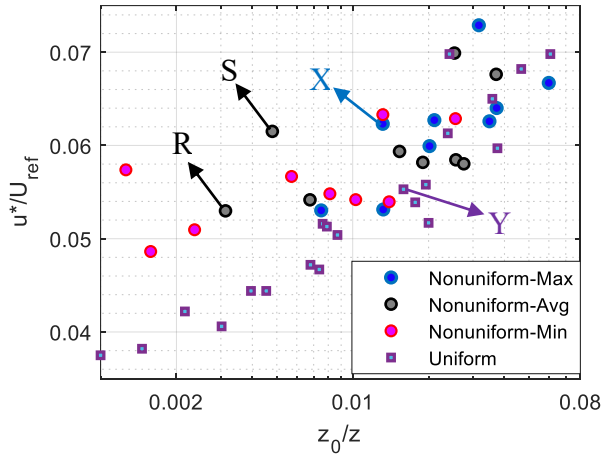

Figure 19 Wind-tunnel friction velocity normalized by U_{ref} for all test cases (nonuniform and uniform) vs. z_0/z from wind-tunnel measurements at z = 10 m full-scale height

Point S shows site 4, Avg case. As shown in Figure 4, for site 4, the height of the roughness element changed from 1.45 cm to 5.45 cm in the immediate upwind of the probe, which led to a sudden increase in the shear stress. Conversely, point R illustrates a sudden decrease (site 1, Avg case). For site 1, in the first subpanel of Figure 4, the height of the roughness element changed from 10 cm to 1.45 cm in the immediate upwind, producing lower friction velocity than the equivalent uniform case. The same concept from the study by Deaves (1981) can be used to explain the difference in the friction velocity of uniform vs. nonuniform cases. Point X represents the normalized friction velocity of site 4 under Max configuration and point Y represents the normalized friction velocity of uniform configuration with H = 4.1 cm. Although the nonuniform case had a slightly smaller z_0 (z_0 = 0.13 m for nonuniform case vs. z_0 = 0.16 m for uniform case),

a sudden increase in the friction velocity was observed since we had a smooth to rough change in the immediate upwind terrain in site 4.

6 Conclusion

When wind-tunnel testing is conducted for the simulation of natural wind flows near the earth's surface, studies to date have simplified a real-world heterogeneous terrain to an upwind fetch of uniform roughness elements. This approach is easier to carry out but may not replicate the true wind characteristics of the site. For example, recent analysis of hurricane wind records over suburban terrains have shown that the field data had a positive non-Gaussian wind speed distribution in the skewness (Balderrama et al., 2012; Fernández-Cabán and Masters, 2017), which would lead to greater gust compared with the Gaussian wind speed distribution from the uniform terrain.

This paper proposes a new method to simulate nonuniform terrains in a wind-tunnel and investigates the wind characteristics produced by the method. To remove the subjectivity, this method first mechanically divides the site into sub-sections with the same characteristics (ex: trees, roads). Next, for each sub-section, the height of the roughness elements is determined using the roughness length of each sub-section. The proposed method is similar to the concept of local roughness zones (Fiedler and Panofsky, 1972; André and Blondin, 1986; Taylor, 1987; Mason, 1988; Vihma and Savijärvi, 1991; Wieringa, 1993; Millward-Hopkins et al., 2011), but also includes a selection of roughness element height within each zone (Macdonald et al., 1998).

The most significant finding was that, unlike conventional uniform configurations, the proposed method produced a non-Gaussian wind speed distribution in the wind-tunnel with positive skewness. However, the skewness was still less than what was observed in the hurricane winds in the field. We also concluded that the skewness profile in the nonuniform representation matched better with the FCMP field measurements.

The other important finding was that — unlike the uniform approximation, the wind characteristics in nonuniform terrain could not be explained by only z_0 values. The other important parameter affecting wind characteristics over nonuniform terrain was the configuration of immediate upwind

terrain. Further analysis of sites showed that wind characteristics such as turbulence intensity, power spectrum, and integral length scale were influenced by the immediate upwind features that did not happen in uniform approximations. When two nonuniform sites had almost the same z_0 estimation, the final patch of upwind terrain near the measurement point was a deciding factor in explaining the differences between the wind characteristics. We also found that nonuniform representation in the sites with rough to smooth immediate upwind change performed better than uniform representation for both mean wind speed and turbulence intensity. The results showed that a rough to smooth change led to an increase in the wind speed and a decrease in turbulence intensity near the ground, and vice versa for a rough to smooth change, when we compare these sites with equivalent uniform cases.

The proposed method and research could help explain the discrepancy between the wind-tunnel results and field observations, but further study is needed to identify the influence of immediate upwind features — unlike the uniform approximation, the proposed nonuniform representation is influenced by the change of roughness in the immediate upwind. In addition, further study is required to show how the nonuniform representation changes the wind loads and pressure distribution on buildings.

Acknowledgment

This material is based upon work supported by the National Science Foundation under Grant No. CMMI-1856205. Any opinions, findings, and conclusions or recommendations expressed in this material are those of the authors and do not necessarily reflect the views of the National Science Foundation. The NSF NHERI Experimental Facility that contributed to the research results reported within this paper was supported under Grant No. CMMI-1520843.

Declarations

Ethical Approval

Not applicable.

Competing interests

The authors declare that they have no known competing financial interests or personal relationships that could have appeared to influence the work reported in this paper.

Authors' contributions

The first, second and third authors prepared the testing matrix. The experimental testing carried out by the first and second authors. The first author contributed to the analysis of the results and to the writing of the manuscripts. The second and fourth authors helped with interpreting the results. All the authors commented on the manuscripts.

Data Availability Statement

The datasets generated (wind tunnel tests dataset) during and used (field measurements dataset) during this study are available from the corresponding author on reasonable requests.

Funding

This material is based upon work supported by the National Science Foundation under Grant No. CMMI-1856205. The NSF NHERI Experimental Facility that contributed to the research results reported within this paper was supported under Grant No. CMMI-1520843.

References

André, J.-C., Blondin, C., 1986. On the effective roughness length for use in numerical three-dimensional models. Boundary-Layer Meteorol. 35, 231–245. https://doi.org/10.1007/BF00123642

ASCE/SEI7-16, 2017. Minimum Design Loads and Associated Criteria for Buildings and Other Structures. American Society of Civil Engineers, Reston, VA. https://doi.org/10.1061/9780784414248

Balderrama, J.A., Masters, F.J., Gurley, K.R., 2012. Peak factor estimation in hurricane surface winds. J. Wind Eng. Ind. Aerodyn. 102, 1–13. https://doi.org/10.1016/j.jweia.2011.12.003

Balderrama, J.A., Masters, F.J., Gurley, K.R., Prevatt, D.O., Aponte-Bermúdez, L.D., Reinhold, T.A., Pinelli, J.-P., Subramanian, C.S., Schiff, S.D., Chowdhury, A.G., 2011. The Florida Coastal Monitoring Program (FCMP): A review. J. Wind Eng. Ind. Aerodyn. 99, 979–995. https://doi.org/10.1016/j.jweia.2011.07.002

Catarelli, R.A., Fernández-Cabán, P.L., Masters, F.J., Bridge, J.A., Gurley, K.R., Matyas, C.J., 2020. Automated terrain generation for precise atmospheric boundary layer simulation in the wind tunnel. J. Wind Eng. Ind. Aerodyn. 207, 104276. https://doi.org/10.1016/j.jweia.2020.104276

Cook, N.J., 1978. Determination of the model scale factor in wind-tunnel simulations of the adiabatic atmospheric boundary layer. J. Wind Eng. Ind. Aerodyn. 2, 311–321. https://doi.org/10.1016/0167-6105(78)90016-8

548 Counihan, J., 1975. Adiabatic atmospheric boundary layers: A review and analysis of data from the period 1880–
549 1972. Atmos. Environ. 9, 871–905. https://doi.org/10.1016/0004-6981(75)90088-8
550 Counihan, J., 1971. Wind tunnel determination of the roughness length as a function of the fetch and the roughness
551 density of three-dimensional roughness elements. Atmos. Environ. Pergamon Press 5, 637–642.
552 https://doi.org/10.1016/0004-6981(71)90120-X
553 Davenport, A.G., 1960. Wind loads on structures, National research council, canads, division of building research.
554 Deaves, D.M., 1981. Computations of wind flow over changes in surface roughness. J. Wind Eng. Ind. Aerodyn. 7,
555 65–94. https://doi.org/10.1016/0167-6105(81)90068-4
556 ESDU, 1974. Characteristics of atmospheric turbulence near the ground. Part I: definitions and general information.
557 Eng. Sci. Data Unit, Itm. No. 7.
558 Farell, C., Iyengar, A.K.S., 1999. Experiments on the wind tunnel simulation of atmospheric boundary layers. J. Wind
559 Eng. Ind. Aerodyn. 79, 11–35. https://doi.org/10.1016/S0167-6105(98)00117-2
560 Fernández-Cabán, P.L., Masters, F.J., 2017. Near surface wind longitudinal velocity positively skews with increasing
561 aerodynamic roughness length. J. Wind Eng. Ind. Aerodyn. 169, 94–105.
562 https://doi.org/10.1016/j.jweia.2017.06.007
563 Ferreira, L.M., Amirinia, G., Jung, S., 2018. Surface pressure distribution on patterned cylinders under simulated
564 atmospheric boundary layer winds. Struct. Des. Tall Spec. Build. 27, e1404. https://doi.org/10.1002/tal.1404
565 Fiedler, F., Panofsky, H.A., 1972. The geostrophic drag coefficient and the 'effective' roughness length. Q. J. R.
566 Meteorol. Soc. 98, 213–220. https://doi.org/10.1002/qj.49709841519
567 Gavanski, E., Uematsu, Y., 2014. Local wind pressures acting on walls of low-rise buildings and comparisons to the
568 Japanese and US wind loading provisions. J. Wind Eng. Ind. Aerodyn. 132, 77–91.
569 https://doi.org/10.1016/j.jweia.2014.06.020
570 Sabareesh, G.A., Matsui, M., Tamura, Y., 2013. Characteristics of internal pressures and net local roof wind forces
571 on a building exposed to a tornado-like vortex. J. Wind Eng. Ind. Aerodyn. 112, 52–57.
572 https://doi.org/10.1016/j.jweia.2012.11.005
573 Gurley, K., F. Masters, T. Reinhold, M. Ojeda, (2021) "Florida Coastal Monitoring Program Hurricanes Report (1999
574 - 2008)", in FCMP Ground Level Hurricane Wind Data (1999 - 2008). DesignSafe-CI.
575 https://doi.org/10.17603/ds2-j82e-nc21 v1
576 He, Y.C., Chan, P.W., Li, Q.S., 2017. Estimation of roughness length at Hong Kong International Airport via different
577 micrometeorological methods. J. Wind Eng. Ind. Aerodyn. 171, 121–136.
578 https://doi.org/10.1016/j.jweia.2017.09.019
579 Ho, T.C.E., Surry, D., Morrish, D., Kopp, G.A., 2005. The UWO contribution to the NIST aerodynamic database for
580 wind loads on low buildings: Part 1. Archiving format and basic aerodynamic data. J. Wind Eng. Ind. Aerodyn.
581 93, 1–30. https://doi.org/10.1016/j.jweia.2004.07.006
582 Jung, S., Masters, F.J., 2013. Characterization of open and suburban boundary layer wind turbulence in 2008
583 Hurricane Ike. Wind Struct. 17, 135–162. https://doi.org/10.12989/was.2013.17.2.135
584 Kopp, G.A., Surry, D., Mans, C., 2005. Wind effects of parapets on low buildings: Part 1. Basic aerodynamics and

local loads. J. Wind Eng. Ind. Aerodyn. 93, 817–841. https://doi.org/10.1016/j.jweia.2005.08.006

Kozmar, H., 2011. Characteristics of natural wind simulations in the TUM boundary layer wind tunnel. Theor. Appl. Climatol. 106, 95–104. https://doi.org/10.1007/s00704-011-0417-9

Kozmar, H., 2010. Scale effects in wind tunnel modeling of an urban atmospheric boundary layer. Theor. Appl. Climatol. 100, 153–162. https://doi.org/10.1007/s00704-009-0156-3

Lettau, H., 1969. Note on Aerodynamic Roughness-Parameter Estimation on the Basis of Roughness-Element Description. J. Appl. Meteorol. 8, 828–832. https://doi.org/10.1175/1520-0450(1969)008<0828:NOARPE>2.0.CO;2

Li, L., Xiao, Y., Kareem, A., Song, L., Qin, P., 2012. Modeling typhoon wind power spectra near sea surface based on measurements in the South China sea. J. Wind Eng. Ind. Aerodyn. 104–106, 565–576. https://doi.org/10.1016/j.jweia.2012.04.005

Lim, H.C., Tsukamoto, K., Ohba, M., Mizutani, K., 2014. Study on the surface pressure distribution of cubes in cross-wind arrays. J. Wind Eng. Ind. Aerodyn. 133, 18–26. https://doi.org/10.1016/j.jweia.2014.07.009

Liu, M., Chen, X., Yang, Q., 2016. Characteristics of dynamic pressures on a saddle type roof in various boundary layer flows. J. Wind Eng. Ind. Aerodyn. 150, 1–14. https://doi.org/10.1016/j.jweia.2015.11.012

Macdonald, R.., Griffiths, R.., Hall, D.., 1998. An improved method for the estimation of surface roughness of obstacle arrays. Atmos. Environ. 32, 1857–1864. https://doi.org/10.1016/S1352-2310(97)00403-2

Mason, P.J., 1988. The formation of areally-averaged roughness lengths. Q. J. R. Meteorol. Soc. 114, 399–420. https://doi.org/10.1002/qj.49711448007

Millward-Hopkins, J.T., Tomlin, A.S., Ma, L., Ingham, D., Pourkashanian, M., 2011. Estimating Aerodynamic Parameters of Urban-Like Surfaces with Heterogeneous Building Heights. Boundary-Layer Meteorol. 141, 443–465. https://doi.org/10.1007/s10546-011-9640-2

Oikawa, S., Meng, Y., 1995. Turbulence characteristics and organized motion in a suburban roughness sublayer. Boundary-Layer Meteorol. 74, 289–312. https://doi.org/10.1007/BF00712122

Panofsky, H.A., Townsend, A.A., 1963. Change of Terrain Roughness and Wind Profile. Q. J. R. Meteorol. Soc. 147–155.

Rizzo, F., D'Asdia, P., Ricciardelli, F., Bartoli, G., 2012. Characterisation of pressure coefficients on hyperbolic paraboloid roofs. J. Wind Eng. Ind. Aerodyn. 102, 61–71. https://doi.org/10.1016/j.jweia.2012.01.003

Sabareesh, G.A., Matsui, M., Tamura, Y., 2013. Characteristics of internal pressures and net local roof wind forces on a building exposed to a tornado-like vortex. J. Wind Eng. Ind. Aerodyn. 112, 52–57. https://doi.org/10.1016/j.jweia.2012.11.005

Shaw, R.H., Seginer, I., 1987. Calculation of velocity skewness in real and artificial plant canopies. Boundary-Layer Meteorol. 39, 315–332. https://doi.org/10.1007/BF00125141

Su, N., Sun, Y., Wu, Y., Shen, S., 2016. three-parameter auto-spectral model of wind pressure for wind-induced response analysis on large-span roofs. J. Wind Eng. Ind. Aerodyn. 158, 139–153. https://doi.org/10.1016/j.jweia.2016.09.013

Taylor, P.A., 1987. Comments and further analysis on effective roughness lengths for use in numerical three-

dimensional models. Boundary-Layer Meteorol. 39, 403–418. https://doi.org/10.1007/BF00125144

Tieleman, H.W., 1995. Universality of velocity spectra. J. Wind Eng. Ind. Aerodyn. 56, 55–69. https://doi.org/10.1016/0167-6105(94)00011-2

Varshney, K., Poddar, K., 2011. Experiments on integral length scale control in atmospheric boundary layer wind tunnel. Theor. Appl. Climatol. 106, 127–137. https://doi.org/10.1007/s00704-011-0415-y

Vihma, T., Savijärvi, H., 1991. On the effective roughness length for heterogeneous terrain. Q. J. R. Meteorol. Soc. 117, 399–407. https://doi.org/10.1002/qj.49711749808

Wang, K., Stathopoulos, T., 2007. Exposure model for wind loading of buildings. J. Wind Eng. Ind. Aerodyn. 95, 1511–1525. https://doi.org/10.1016/j.jweia.2007.02.016

Wang, K., Stathopoulos, T., 2006. The impact of exposure on wind loading of low buildings. Proc. Struct. Congr. Expo. 2006, 9. https://doi.org/10.1061/40889(201)9

Weber, R.O., 1999. Remarks on the Definition and Estimation of Friction Velocity. Boundary-Layer Meteorol. 93, 197–209. https://doi.org/10.1023/A:1002043826623

Wiernga, J., 1993. Representative roughness parameters for homogeneous terrain. Boundary-Layer Meteorol. 63, 323–363. https://doi.org/10.1007/BF00705357

Xiao, M.Y., Hong, H.P., 2022. Modeling Nonstationary Non-Gaussian Hurricane Wind Velocity and Gust Factor. J. Struct. Eng. 148. https://doi.org/10.1061/(ASCE)ST.1943-541X.0003243

Zisis, I., Stathopoulos, T., 2010. Wind loads on low-rise buildings: Upstream exposure effect. 7th Asia-Pacific Conf. Wind Eng.